BMC Medicine

RESEARCH

Open Access

Cilnidipine exerts antiviral effects in vitro and in vivo by inhibiting the internalization and fusion of influenza A virus

Yinyan Li[1,2], Sizu Yang[2], Feng Jiang[2], Siqi Luo[2], Jinlong Liang[2], Linrui Jiang[2], Zhixuan Chen[2], Xin Chen[1*] and Jie Yang[2*]

Abstract

Background Influenza A virus (IAV) is a major cause of seasonal and global pandemics, posing serious health risks. Repositioning approved drugs offers an efficient antiviral strategy, particularly as calcium (Ca^{2+}) is crucial for IAV infection, making Ca^{2+} channel blockers (CCBs) promising candidates for antiviral agents.

Methods The in vitro antiviral activity of cilnidipine was evaluated using MTT assays, qRT-PCR, plaque assays, and western blotting. Mechanistic studies involved time-of-addition, viral internalization, pseudovirus neutralization, and HA (hemagglutinin) syncytium assays. For in vivo analysis, BALB/c mice were intranasally infected to evaluate the effects of cilnidipine on viral titer, lung index, pulmonary inflammatory mediators, and survival rate.

Results In vitro, cilnidipine exhibits antiviral activity against IAV during the early stages of infection. It disrupts clathrin- and caveolin-mediated endocytosis to inhibit the internalization of IAV and interacts with the viral HA2 subunit to impede virus membrane fusion. Additionally, cilnidipine suppresses the PI3K-AKT and p38 MAPK pathways activated by IAV infections. In vivo, cilnidipine reduces virus titers and lung index, ameliorates lung pathology, and inhibits pulmonary inflammatory mediator expression, improving survival rates.

Conclusions These findings highlight the promising anti-IAV properties of cilnidipine both in vitro and in vivo, suggesting its potential as a clinical agent for emergencies against influenza outbreaks.

Keywords Antiviral activity, Influenza A virus, Cilnidipine, Entry inhibitor, Internalization, Drug repositioning

Background

Influenza A virus (IAV) can rapidly evolve through antigenic drift and antigenic shift, leading to outbreaks of acute respiratory disease in both domestic poultry and humans [1, 2]. This evolution has resulted in significant challenges, such as the emergence of pandemic H1N1 influenza in 2009, human infections with avian H7N9 influenza in 2013, and sporadic human cases of highly pathogenic avian H5N1 influenza (HPAI) [3–6]. Vaccination remains the most effective way to prevent and control influenza; however, regular updates are necessary to address the evolving nature of the virus, which can result in increased economic burdens [7, 8]. Despite the

*Correspondence:
Xin Chen
chen_xin1020@163.com
Jie Yang
yj528@smu.edu.cn
[1] Department of Pulmonary and Critical Care Medicine, Zhujiang Hospital, Southern Medical University, Guangzhou, China
[2] NMPA Key Laboratory for Research and Evaluation of Drug Metabolism, Guangdong Provincial Key Laboratory of New Drug Screening, Guangdong-Hongkong-Macao Joint Laboratory for New Drug Screening, School of Pharmaceutical Sciences, Southern Medical University, Guangzhou, China

availability of antiviral drugs, their efficacy is limited due to resistance and side effects. The Centers for Disease Control and Prevention (CDC) has approved four antiviral medications for treating circulating influenza strains, including three neuraminidase inhibitors (NAIs): peramivir, zanamivir, and oseltamivir phosphate, as well as baloxavir marboxil [9, 10]. NAIs, which block viral neuraminidase (NA) to inhibit progeny virus release, have been effective but face challenges from resistance due to mutations in the NA gene [11]. This concern was heightened following the global spread of oseltamivir-resistant seasonal H1N1 influenza viruses from 2007–2009 [12, 13]. Similarly, baloxavir, a novel antiviral medication that inhibits the endonuclease activity of the polymerase acidic (PA) protein to impede viral RNA synthesis, has also faced challenges with the emergence of treatment-resistant strains during clinical trials [14, 15]. Consequently, there is an urgent need for innovative strategies to combat influenza infections, and drug repurposing has emerged as a promising and efficient approach.

Blocking viral entry represents an effective approach for developing antiviral therapies [16–18]. IAV infection begins with the virus attaching to host cells, followed by endocytosis and the formation of an endosome encapsulating the virus particles [19]. The viral membrane then fuses with the host membrane, releasing the RNA genome into the nucleus to initiate transcription and replication [20, 21]. Calcium (Ca^{2+}) plays a critical role in multiple stages of viral infection, including viral entry, gene replication, virion maturation, and release, significantly contributing to the pathogenesis of various viruses [22, 23]. Fujioka et al. found that influenza hemagglutinin (HA) binds to the voltage-dependent Ca^{2+} channels (VDCCs) Cav1.2, inducing intracellular Ca^{2+} oscillations that facilitate IAV entry and replication [24]. Importantly, IAV entry was inhibited by calcium channel blockers (CCBs) or through the knockdown of Cav1.2 expression [24]. Therefore, CCBs may serve as viral entry inhibitors to effectively target the initial stages of infection. Previous studies have indicated that the L-type Ca^{2+} channel inhibitor benidipine hydrochloride inhibits severe fever with thrombocytopenia syndrome virus (SFTSV) by impeding virus internalization and reducing viral genome replication [25]. Similarly, diltiazem, another L-type Ca^{2+} channel inhibitor, has demonstrated efficacy against SARS-CoV-2 by inhibiting viral attachment and internalization [26]. Additionally, CCBs such as verapamil, diltiazem, and BAPTA-AM have shown effectiveness against influenza virus infection both in vitro and in vivo [24, 27, 28]. These findings provide new perspectives for treating viral infections, highlighting the potential of targeting Ca^{2+} channels to impede viral entry and suggesting CCBs as a promising class of antiviral therapeutic agents. Furthermore, repurposing host-targeted drugs like CCBs offers a rapid and practical approach to identifying new antiviral treatments, a critical advantage in addressing emerging outbreaks or pandemics with limited therapeutic options.

This research examines the in vivo and in vitro antiviral activity of cilnidipine against IAV and elucidates its mechanism of action. The results highlight the potential of cilnidipine as a therapeutic option for combating IAV infection, highlighting Ca^{2+} channels as promising targets for future antiviral drug development strategies.

Methods

Reagents and antibodies

Cilnidipine (T0388) with 98% purity was purchased from Target Molecule Corp. (Shanghai, China). Ribavirin, 3-(4,5-dimethylthiazol-2-yl)−2,5-diphenyltetrazolium bromide (MTT), carboxymethyl cellulose sodium salt (CMC), TPCK-trypsin, methyl-β-cyclodextrin (MβCD), and oseltamivir were all purchased from Sigma–Aldrich (Saint Louis, MO, USA). Oseltamivir phosphate (Ose) was obtained from Hoffmann-La Roche (Basel, Switzerland). CL-385319, 98% pure, was synthesized in our laboratory. Arbidol was purchased from Weikeqi (Sichuan, China). Alexa 568-conjugated human transferrin (Tf-568) was purchased from Invitrogen (T23365, Carlsbad, CA, USA). FITC-conjugated cholera toxin beta-subunit (CTB-FITC) was also purchased from Sigma–Aldrich (Saint Louis, MO, USA). Chlorpromazine (CPZ) was purchased from Aladdin (Shanghai, China). Cepharanthine (CEP), with a purity of 97%, was purchased from Bidepharm (Shanghai, China).

The following antibodies were used: anti-NP monoclonal antibody (GeneTex, GTX125989), anti-PB2 monoclonal antibody (GeneTex, GTX125926), anti-GAPDH polyclonal antibody (Bioss, bs-2188R), anti-rabbit/mouse horseradish peroxidase (HRP)-conjugated secondary antibody (Fdbio Science, FDR007, FDM007), AlexaFluor 488-conjugated anti-rabbit IgG antibody (Abcam, ab150077), anti-AKT1 monoclonal antibody (ZenBio, R380617), anti-phospho-AKT (Ser473) polyclonal antibody (ZenBio, 310,021), anti-phospho-PI3 kinase p85/p55 (Tyr467/Tyr199) polyclonal antibody (ZenBio, 341,468), anti-PI3 kinase p85 alpha (1C8) polyclonal antibody (ZenBio, 251,221), anti-p38 monoclonal antibody (ZenBio, R27123), anti-phospho-p38 (Tyr182) polyclonal antibody (ZenBio, 310,069), anti-transferrin antibody (Bioss, bs-33244 M), and anti-caveolin-1 antibody (Bioss, bs-1453R).

Cells and viruses

Madin–Darby canine kidney (MDCK), human lung epithelial (A549), and human embryonic kidney (HEK293T)

cells were obtained from the American Type Culture Collection (ATCC, Manassas, VA, USA). All the cells were cultured in Dulbecco's modified Eagle's medium (DMEM, Gibco, Carlsbad, CA, USA) supplemented with 10% fetal bovine serum (FBS, ExCellBio, Shanghai, China) and 1% penicillin/streptomycin (Gibco, Carlsbad, CA, USA) at 37 °C with 5% CO_2. IAV strains, including A/Puerto Rico/8/34 (H1N1), A/FM-1/1/47 (H1N1), A/WSN/33 (H1N1), A/PR/8/34 with NA-H274Y, A/Aichi/2/68 (H3N2) and a mouse-adapted strain of A/PR/8/34 virus, were propagated in SPF embryonated chicken eggs. The virus titer was determined by analyzing the 50% tissue culture infective dose ($TCID_{50}$) via the Reed–Muench assay [29].

MTT assay

The MTT assay was used to evaluate cytotoxicity and anti-IAV activity, and GraphPad Prism 8.0 software was used to determine the CC_{50} and IC_{50} values. For the cytotoxicity assay, cilnidipine was serially diluted twofold in 96-well plates containing 10,000 cells *per* well, followed by a 48 h incubation at 37 °C. For the antiviral assay, MDCK cells were pretreated with cilnidipine for 2 h and then infected with IAV ($100TCID_{50}$) for 1 h at 37 °C. Post-infection, the viral supernatant was removed, and cilnidipine was added at a twofold dilution in serum-free DMEM supplemented with TPCK-trypsin (1 μg/mL), followed by a 48 h incubation at 37 °C. The virus-induced cytopathic effect (CPE) was observed and documented via microscopy (Nikon, Tokyo, Japan). The supernatant was subsequently aspirated, and MTT solution (0.5 mg/mL) in serum-free DMEM was added, followed by a 4 h incubation at 37 °C in the dark. The formazan crystals were dissolved in dimethyl sulfoxide (DMSO, Aladdin, Shanghai, China), and absorbance readings were taken at 570 nm via a microplate reader (GENios Pro, TECAN, Bedford, MA, USA).

Western blot

A549 cells were pre-incubated with cilnidipine for 2 h before infection with IAV (MOI = 0.1) at 37 °C for 1 h. Subsequently, the viral supernatant was removed, and cilnidipine was added to serum-free DMEM at a twofold dilution and incubated at 37 °C for 24 h. Cell lysis was performed using RIPA buffer (Fdbio Science, Hangzhou, China) to extract proteins. The proteins were denatured by boiling at 105 °C for 15 min after adding loading buffer (5×). Proteins were separated based on their molecular weights via sodium dodecyl sulfate–polyacrylamide gel electrophoresis (SDS–PAGE). The proteins were then transferred onto polyvinylidene fluoride (PVDF) membranes (Roche, Basel, Switzerland) via the wet transfer method at 100 V for 70 min. The PVDF membrane was blocked with 5% skim milk (Fdbio Science, Hangzhou, China) at room temperature (RT) for 1 h, followed by overnight incubation with the primary antibody at 4 °C. After washing three times with Tris-buffered saline-0.1% Tween 20 (TBST), the membranes were incubated with secondary antibodies at RT for 1 h. After three washes with TBST, images were captured via a FluorChem E imaging system (ProteinSimple, CA, USA) and analysed via ImageJ software (NIH, Bethesda, MD, USA).

Quantitative real-time PCR (qRT–PCR)

Antiviral experiments were performed as described above. RNA extraction from cells or mouse lung tissues was carried out via a total RNA isolation kit (Foregene, Chengdu, China). The extracted RNA was subsequently reverse transcribed into cDNA via a PrimeScript RT reagent kit (Takara, Otsu, Shiga, Japan) on a T100 Thermal Cycler (Bio-Rad, Hercules, CA, USA). Quantitative polymerase chain reaction (qPCR) was performed via real-time Applied Biosystems StepOne software (Thermo Fisher Scientific, Waltham, MA, USA) with SYBR Green qPCR Master Mix (Vazyme, Nanjing, China) following the manufacturer's instructions. The relative mRNA expression levels were determined via the $2^{-\Delta\Delta CT}$ method, with all values normalized to the GAPDH level. The primers used in the study were synthesized by Tsingke Biotech Co., Ltd. (Beijing, China).

Indirect immunofluorescence assay

MDCK cells were seeded at a density of 1×10^5 cells/mL in 48-well plates and incubated overnight. The cells were pretreated with cilnidipine at 37 °C for 2 h, followed by infection with WSN virus (MOI = 0.01) at 37 °C for 1 h. The viral supernatant was aspirated, and serum-free DMEM containing 1 μg/mL TPCK-trypsin supplemented with cilnidipine was added for 24 h. Subsequently, the MDCK cells were fixed in 4% paraformaldehyde (PFA, Biosharp, Hefei, China) for 15 min, permeabilized with 0.1% Triton X-100 (Aladdin, Shanghai, China) for 10 min, and then incubated with 5% bovine serum albumin (BSA, Biofroxx, Frankfurt, Germany) at RT for 1 h. Following a wash with PBST (0.05% Tween 20), the cells were incubated with anti-IAV NP antibody (1:500 dilution) and AlexaFluor 488-conjugated anti-rabbit IgG antibody (1:500 dilution). Nuclei were stained with Hoechst 33342 (Beyotime, Shanghai, China). Finally, the cells were washed with PBST and examined via a Ti-Eclipse inverted fluorescence microscope (Nikon, Tokyo, Japan).

Plaque assay

Serial dilutions of supernatants from infected A549 cells or mouse lung homogenates were added to MDCK cell monolayers and incubated for 1 h at 37 °C. After

the supernatant was removed, an equivalent volume of 2×DMEM (EallBio, Beijing, China) and microcrystalline cellulose containing 1 μg/mL TPCK-trypsin were added. After 48 h of incubation, the cells were fixed with 4% paraformaldehyde (PFA) for 20 min and stained with 2% crystal violet (Sigma–Aldrich, Saint Louis, MO, USA) for 15 min. Visualization was performed via ELISPOT S6 Versa (CTL, Cleveland, OH, USA).

Tine-of-addition assay

A549 cells were seeded into 12-well plates at a density of 2×10^5 cells/mL and cultured overnight. Subsequently, the A549 cells were washed twice with PBS and infected with WSN virus (MOI = 0.1) for 1 h at 37 °C. Cilnidipine (20 μM) was administered at intervals of 0–2, 2–5, 5–8, 8–10 and 0–10 h post infection (h p.i.). Protein samples were collected at 10 h p.i. via RIPA buffer for western blot analysis.

Ammonium chloride (NH_4Cl) inhibition assay

A549 cells were pretreated with cilnidipine for 2 h at 37 °C. The cells were subsequently incubated with WSN (MOI = 5) for 1 h at 4 °C. After the viral supernatant was removed, it was replaced with DMEM containing 50 mM NH_4Cl and the indicated concentrations of cilnidipine. Following incubation at 37 °C for 24 h, RNA extraction was performed to determine the NP mRNA levels via qRT–PCR, as previously described.

Viral internalization assay

A549 cells were pretreated with cilnidipine (20 μM) for 2 h at 37 °C, followed by infection with WSN virus (MOI = 5) for 1 h at 4 °C. Unbound viral particles were subsequently removed by washing the cells with pre–cooled PBS, and the cells were then transferred to 37 °C for 0.5 h and 1 h to induce internalization. After 0.5 h or 1 h, the cells were treated with 0.25% EDTA-trypsin (Gibco, Carlsbad, CA, USA) to remove the noninternalized virus. The levels of viral NP RNA and protein in the cell lysates were quantified via qRT–PCR and western blotting, respectively.

Acidification induced membrane fusion assay

A549 cells were pretreated with compounds for 2 h at 37 °C and then infected with WSN virus (MOI = 5) for 1 h at 4 °C. The cells were subsequently treated with PBS-HCl (pH = 5.0) for 10 min at 37 °C to facilitate virion fusion. After that, the supernatant was removed, and DMEM containing the compounds was added, followed by incubation at 37 °C for 6 h. Finally, the cells were lysed in RIPA buffer and analysed by western blotting as described above.

Entry inhibition assays of H5N1 pseudotypes

The H5N1 pseudoviruses were generated as previously described [30]. Briefly, 293T cells were co-transfected with HA plasmids (Thailand-HA, Qinghai-HA or Anhui-HA), A/Thailand/Kan353/2004-NA plasmids, and pNL4-3.luc. R − E − using the PEI reagent. After 48 h of transfection, the culture supernatants were harvested and stored at − 80 °C. Furthermore, MDCK cells were seeded in 96-well plates and grown overnight. Equal volumes of cilnidipine at the indicated concentrations were incubated with H5N1 pseudovirus at 37 °C for 30 min before being added to MDCK cells, which were further incubated for an additional 48 h. MDCK cells were washed with PBS and lysed with lysis reagent (Promega, Madison, WI). A luciferase assay system (Promega, Madison, WI) was subsequently used to measure fluorescence in a microplate reader (GENiosPro, TECAN, Bedford, MA, USA).

HA syncytium assay

MDCK cells were transfected with the A/Thailand/Kan353/2004-HA plasmid (2 μg *per* well) using PEI transfection reagent (4 μL *per* well). After 48 h of transfection, the HA protein was initially cleaved by incubation with 5 μg/mL TPCK-trypsin for 15 min at 37 °C. The cells were subsequently preincubated with cilnidipine for 15 min at 37 °C and then incubated with pH 5.0 PBS for another 15 min at 37 °C. Following washing with PBS, the cells were supplemented with DMEM containing 10% FBS and subsequently incubated for an additional 4 h at 37 °C. Finally, the cells were then fixed with 4% PFA for 20 min, stained with Giemsa (Ding Guo Chang Sheng Biotechnology Co., Ltd, Beijing, China), and observed under a microscope (Nikon, Tokyo, Japan).

Surface plasmon resonance (SPR) assay

The binding of cilnidipine to the HA2 protein was studied via the PlexArray® HT system (Plexera® Bioscience, Seattle, WA, USA). Influenza HA2 protein (Sino Biological, China) was immobilized onto the surface of a 3D Dextran chip. Subsequently, cilnidipine was diluted in PBS at various concentrations as analytes, and PBS was used as running buffer. For binding studies, analytes were applied at corresponding concentrations in running buffer at a flow rate of 2 μL/s with a contact time of 300 s and a dissociation time of 300 s. Chip platforms were regenerated with regeneration buffer (Glycine–HCl, pH = 2.0) after each test cycle. The data were analysed using BIAevaluation Software (BiaCore, Uppsala, Sweden).

Transferrin absorption inhibition assay

As previously reported [31], A549 cells were seeded into 6-well plates at 37 °C and pretreated with cilnidipine for 2 h. Subsequently, the cells were incubated with 2 μg /mL of transferrin (Solarbio, Beijing, China) for 1 h at 4 °C. Unbound transferrin was removed by washing the cells twice with PBS, followed by a 1 h incubation at 37 °C to facilitate the internalization of transferrin. Uninternalized transferrin was removed via 0.25% EDTA-Trypsin. The cells were then lysed in RIPA buffer, and western blot analysis was conducted as described above.

Caveolin-1 inhibition assay

A549 cells were seeded into 6-well plates at 37 °C and pretreated with cilnidipine for 2 h, followed by infection with WSN (MOI = 5) at 4 °C for 1 h. Subsequently, the cells were shifted to 37 °C and incubated for 1 h. Caveolin-1 protein levels were subsequently assessed via western blot analysis as described above.

Fluorescence confocal assays

As previously reported, A549 cells were seeded in 35 mm confocal dishes (Cellvis, CA, USA) for visualization of transferrin uptake via immunofluorescence [32]. A549 cells were subsequently pretreated with test compounds at 37 °C for 2 h, followed by a 1 h incubation at 4 °C with Tf-568 (25 μg/mL) or CTB-FITC (2 μg/mL). Afterward, internalization was allowed to occur during another 15 min of incubation at 37 °C. Once internalized, the cells were fixed with 4% PFA for 15 min and then washed with PBS before being visualized via confocal microscopy (Zeiss LSM800, Oberkochen, Germany).

Animal experiments

SPF female and male BALB/c mice (4–5 weeks old; 16–18 g) were purchased from the Laboratory Animal Center of Southern Medical University (Guangzhou, China). All the mice were randomly divided into 6 groups: the blank group, PR8 virus group, PR8 virus + cilnidipine high-dose group (50 mg/kg/d), PR8 virus + cilnidipine middle-dose group (25 mg/kg/d), PR8 virus + cilnidipine low-dose group (12.5 mg/kg/d), and PR8 virus + Ose group (60 mg/kg/d). Cilnidipine and Ose were dissolved in a 0.5% CMC solution and administered orally. The blood pressure of the mice was assessed via a noninvasive blood pressure monitor (BP-2010A, Softron, Beijing, China) both before and after cilnidipine treatment. The mice were anesthetized with isoflurane (RWD Life Science, Shenzhen, China) and intranasally infected with 50 μL of the PR8 virus *per* mouse. Cilnidipine and Ose were administered for 2 days before PR8 virus infection on day 0, which was continuously administered for 5 days, and mouse lung tissues were harvested and weighed at 5 days post-infection (d p.i.). The lung index was calculated as the ratio of the lung weight (mg) to the body weight (g). Subsequently, the lung tissues were homogenized in PBS for viral titer assessment via a plaque assay and the Reed-Muench method. Hematoxylin–eosin (H&E) staining was used to detect pathological alterations in the lung tissues, whereas qRT–PCR was used to quantify the mRNA expression levels of NP and inflammatory factors in the lung tissues. For survival experiments, the mice were continuously administered cilnidipine and Ose for 7 days, and their body weights and survival rates were monitored for 14 days after PR8 virus infection.

Statistical analysis

All the data were statistically analysed via GraphPad Prism 8.0 (GraphPad Software, La Jolla, CA, USA). The results are presented as the means ± standard deviations (SDs). For comparisons involving more than two groups, one-way analysis of variance (ANOVA) was employed. Levels of statistical significance were considered as follows: * $p < 0.05$, ** $p < 0.01$ and *** $p < 0.001$.

Results

Cilnidipine exhibits anti-influenza virus activity in vitro

Our previous study successfully identified several compounds with activity against IAV from a library of 361 ion channel inhibitors [33]. Among them, the dihydropyridine Ca^{2+} channel inhibitor cilnidipine exhibited inhibitory activity against various strains of IAV, with a 50% maximal inhibitory concentration (IC_{50}) ranging from 3.67 to 7.43 μM (Table 1). The 50% cytotoxic concentration (CC_{50}) in MDCK cells exceeded 200 μM, with a selectivity index greater than 26. Oseltamivir and ribavirin were used as positive controls. Notably, cilnidipine also had a strong antiviral effect on the oseltamivir-resistant strains with a mutation at position 274 of the NA gene, with an IC_{50} value of 4.74 μM (Table 1). We further investigated the inhibitory effect and antiviral mechanism of cilnidipine using the A/WSN/1933 (H1N1) strain due to its high titer and stability.

Following WSN infection, MDCK cells exhibited a noticeable cytopathic effect (CPE), characterized by cellular shrinkage, rounding and shedding. However, treatment with cilnidipine effectively mitigated WSN-induced CPE and maintained cellular integrity (Fig. 1A). To further investigate the antiviral effects of cilnidipine, western blot and qRT-PCR were performed, revealing that cilnidipine successfully suppressed the expression of the virus NP protein and mRNA (Fig. 1B and 1C). Consistent with the above findings, the green fluorescence indicative of NP protein expression showed a similar reduction following cilnidipine treatment (Fig. 1D). To assess the

Table 1 Inhibitory effects of cilnidipine on different IAV subtypes

Compound	IAV strains	[a] IC_{50} (μM)	CC_{50} (μM)	[b] SI
Cilnidipine	A/Puerto Rico/8/34 (H1N1)	5.74 ± 0.99	> 200	> 34.84
	A/Aichi/2/68 (H3N2)	7.43 ± 1.62		> 26.92
	A/WSN/1933 (H1N1)	6.42 ± 1.19		> 31.15
	A/FM1/1/47 (H1N1)	4.74 ± 1.52		> 42.19
	[c] A/PR/8/34 (H1N1) with the NA-H274Y	3.67 ± 0.98		> 54.50
[d] Ribavirin	A/WSN/1933 (H1N1)	4.82 ± 1.43		> 41.49
[e] Oseltamivir	A/WSN/1933 (H1N1)	0.87 ± 0.39		> 229.89

[a] IC_{50}: half maximal inhibitory concentration

[b] SI (selectivity index) = CC_{50}/IC_{50}

[c] Oseltamivir-resistant strain

[d, e] Positive control

The data are presented as the means ± SDs

impact of cilnidipine on progeny viral production, the supernatant collected from WSN-infected A549 cells at 24 h p.i. was used for the plaque assay. As shown in Fig. 1E, cilnidipine significantly reduced progeny virus titers in the supernatant. In summary, cilnidipine exhibits promising inhibitory effects against IAV infection in vitro, suggesting its potential for further development and optimization as an antiviral agent.

Cilnidipine inhibits IAV infection by interfering with virus internalization and membrane fusion

In a single-cycle replication of IAV infection, cilnidipine was administered at various time intervals, with protein samples collected at 10 h p.i. for western blotting (Additional file 1: Fig S1) [34]. The results revealed significant inhibition of NP protein expression at 0–2 h, suggesting that cilnidipine plays a crucial role during the viral entry stage (Fig. 2A). To further evaluate its effect on viral entry, A549 cells were pre-incubated with cilnidipine and exposed to the virus at 4℃ for 1 h, followed by replacement of the supernatant with fresh medium containing ammonium chloride (NH_4Cl) to prevent membrane fusion. The results showed that cilnidipine reduced viral NP mRNA expression in the presence of NH_4Cl, suggesting antiviral activity before membrane fusion (Fig. 2B). The binding assay demonstrated that cilnidipine did not inhibit the expression of viral NP protein at 4 °C and therefore did not affect viral binding to cells (Additional file 1: Fig. S2). A549 cells were exposed to WSN virus at 4℃ and then transferred to 37℃ for 0.5 and 1 h to allow internalization. Uninternalized viral particles were removed using 0.25% EDTA-trypsin (Additional file 1: Fig. S3), viral NP protein and mRNA expression were subsequently measured. The results demonstrated that cilnidipine effectively inhibited virus internalization at both 0.5 h and 1 h, reducing NP mRNA and protein expression (Fig. 2C and 2D). At pH 5.0, virus-cell membrane fusion is directly induced, bypassing endocytosis. Cepharanthine (CEP) targets viral ribonucleoprotein complexes (VRNPs) to inhibit viral NP protein expression, without affecting endocytosis (Fig. 2E) [35]. However, cilnidipine and CPZ did not show inhibitory effects, suggesting that the internalization phase is the primary requirement for cilnidipine action (Fig. 2E). These findings indicate that cilnidipine is an effective inhibitor of influenza virus internalization.

The HA and NA proteins located on the envelope of influenza viruses are essential for facilitating viral entry and release. To examine the effect of cilnidipine on viral envelope proteins, HA and NA plasmids were transfected into 293T cells to construct H5N1 pseudoviruses, as detailed in a previous study [30]. Cilnidipine treatment effectively suppressed H5N1 pseudovirus infection in MDCK cells but had no effect on the VSV-G negative control (Fig. 2F). CL-385319 was used as a positive control (Additional file 1: Fig. S4) [30]. These findings suggest that cilnidipine interferes with the function of either HA or NA proteins. However, the results of the MU-NANA inhibition assay revealed that cilnidipine did not inhibit NA activity, in contrast to zanamivir, which exhibited concentration-dependent inhibition of NA activity (Additional file 1: Fig. S5). Consequently, cilnidipine might specifically target the viral HA protein, which consists of the HA1 and HA2 subunits. While cilnidipine showed no inhibitory effect on IAV-induced red blood cell aggregation (Additional file 1: Fig. S6), it significantly attenuated pH 5.0-dependent syncytium formation in HA-expressing MDCK cells (Fig. 2G), demonstrating its specific antagonism of HA2-mediated membrane fusion. To confirm this interaction, the binding affinity between cilnidipine and the HA2 protein was further validated by SPR assay, with a KD value of 3.2×10^{-8} M

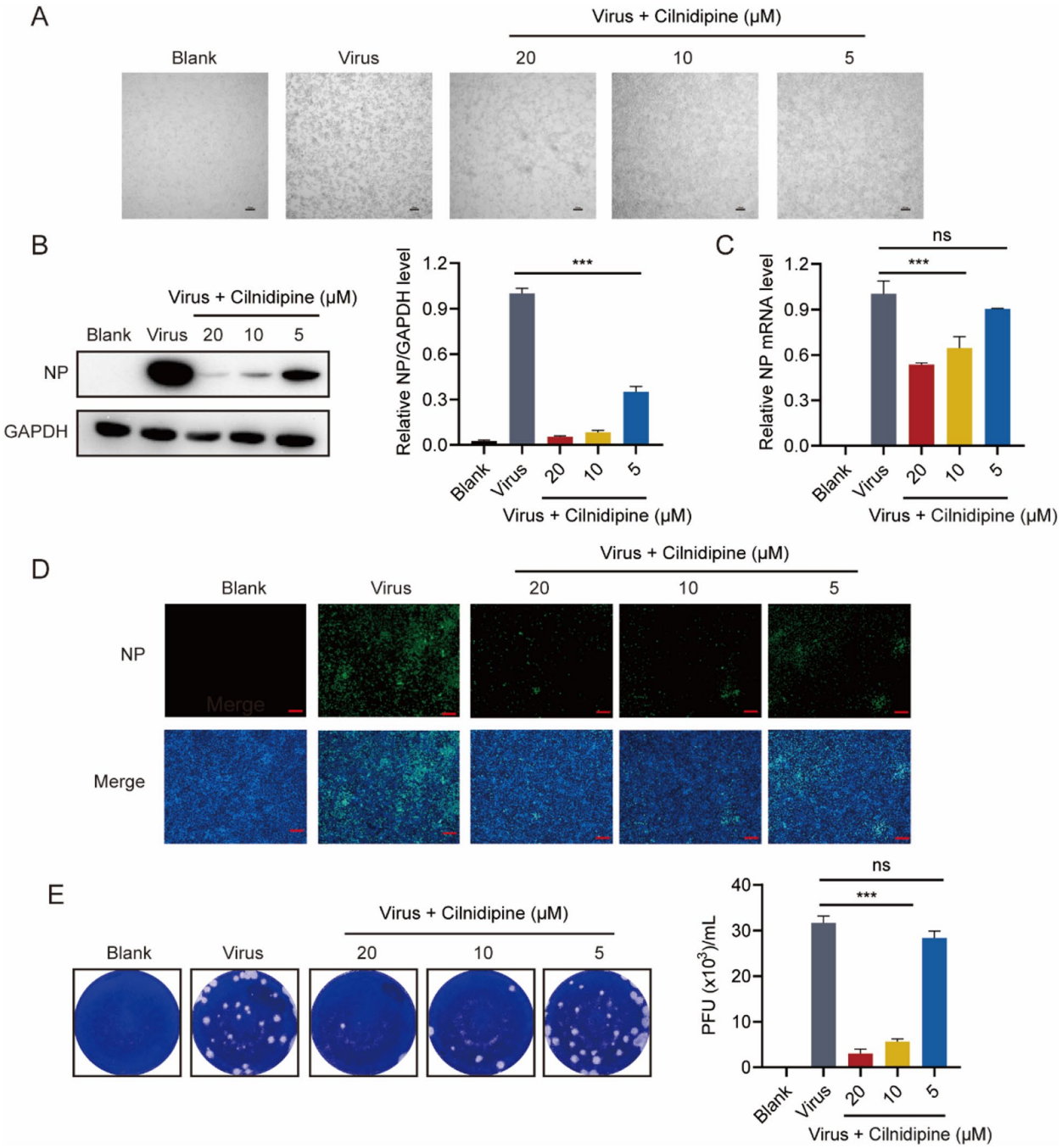

Fig. 1 The inhibitory effect of cilnidipine on IAV infection was evaluated in vitro. **A** Microscopic observation (100×) of the inhibitory effect of cilnidipine on WSN-induced CPE in MDCK cells. Scale bar: 100 μm. **B**–**C** The inhibitory effect of cilnidipine on the expression of NP protein and mRNA in WSN-infected A549 cells was detected by western blotting and qRT-PCR, respectively. **D** The inhibitory effect of cilnidipine on the expression of the viral NP protein was detected via indirect immunofluorescence (100×). The NP protein was visualized as green fluorescence, whereas the nucleus was stained blue. Scale bar: 100 μm. **E** Viral titers in the supernatants of WSN-infected A549 cells were quantified via a plaque assay, with the supernatant diluted 1000-fold. Data are presented as means ± SDs, *** $p < 0.001$, ns means not significant

(Fig. 2H). Furthermore, the mini-replicon assay revealed that cilnidipine did not inhibit vRNP activity (Additional file 1: Fig. S7).

Cilnidipine inhibits clathrin-mediated and caveolin-mediated endocytosis of influenza virus

In this study, we examined the inhibitory effect of

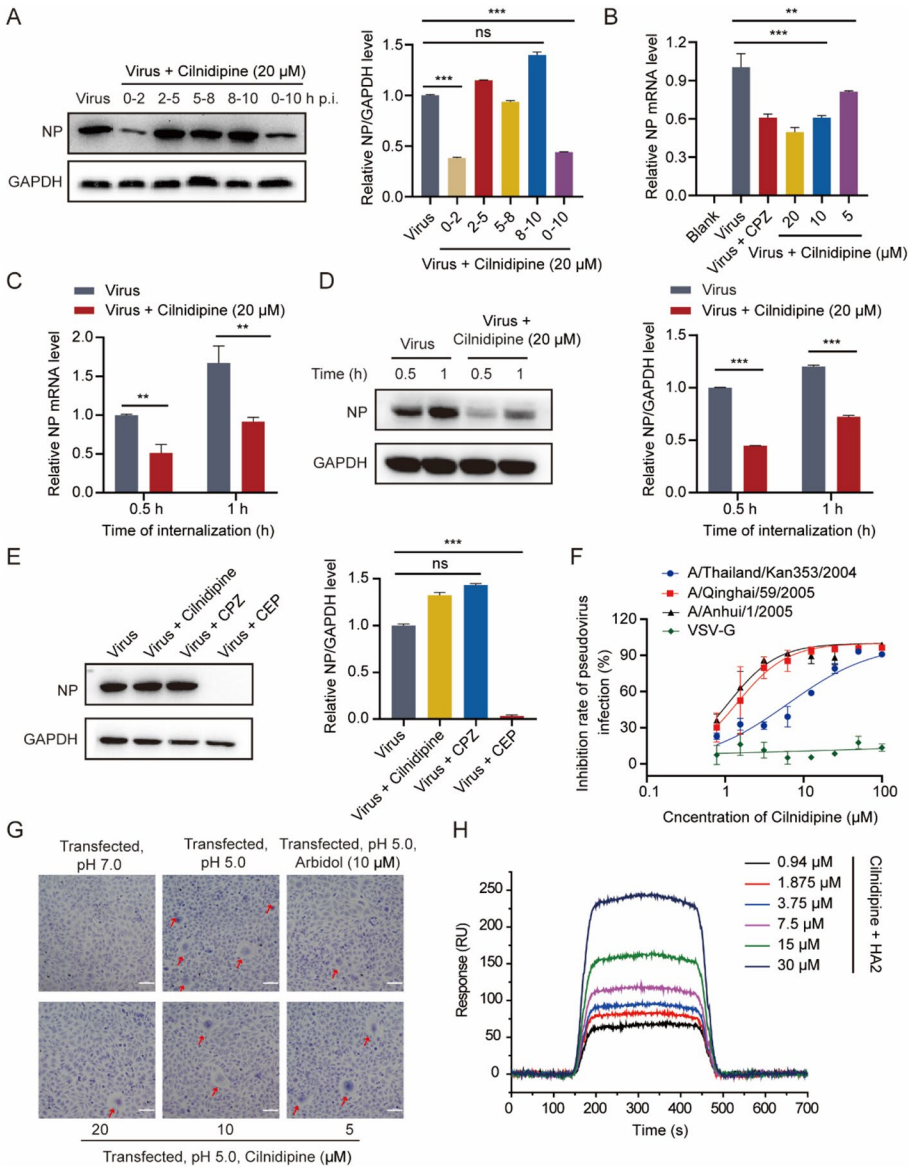

Fig. 2 Cilnidipine exerts antiviral effects by inhibiting viral internalization and membrane fusion. **A** A549 cells infected with WSN virus were treated with cilnidipine (20 μM) at different time intervals (0–2, 2–5, 5–8, 8–10 and 0–10 h) to detect the expression of the viral NP protein. **B** The effect of cilnidipine on the pre–fusion stage of the virus was investigated in A549 cells in the presence of NH_4Cl. CPZ (20 μM) was used as positive control. **C–D** The effect of cilnidipine on NP mRNA and protein expression during virus internalization was measured by qRT–PCR and western blotting, respectively. **E** The antiviral effect of cilnidipine was assessed by directly inducing membrane fusion at pH 5.0 to bypass the internalization. **F** The inhibitory effect of cilnidipine on H5N1 pseudoviruses packaged with HA and NA plasmids was evaluated in MDCK cells. **G** The effect of cilnidipine on membrane fusion was evaluated by detecting polykaryon formation in MDCK cells transfected with the HA plasmid at pH 5.0 (200×). Scale bar: 100 μm. **H** An SPR assay was used to detect the binding affinity between cilnidipine and the HA2 protein. The data are presented as the means ± SDs, ** $p < 0.01$, *** $p < 0.001$, ns means not significant

cilnidipine on both clathrin-mediated endocytosis (CME) and caveolin-mediated endocytosis. After incubating cells with transferrin, a specific marker for CME, we observed that transferrin uptake decreased with increasing concentrations of cilnidipine, indicating disruption of CME (Fig. 3A). For further confirmation, a direct fluorescence assay was employed using Tf-568 (25 μg/mL) to visualize transferrin localization in A549 cells. Treatment with cilnidipine and CPZ (20 μM) resulted in reduced diffuse fluorescence surrounding the cells, confirming effective inhibition of transferrin internalization (Fig. 3B). Additionally, we investigated the impact of

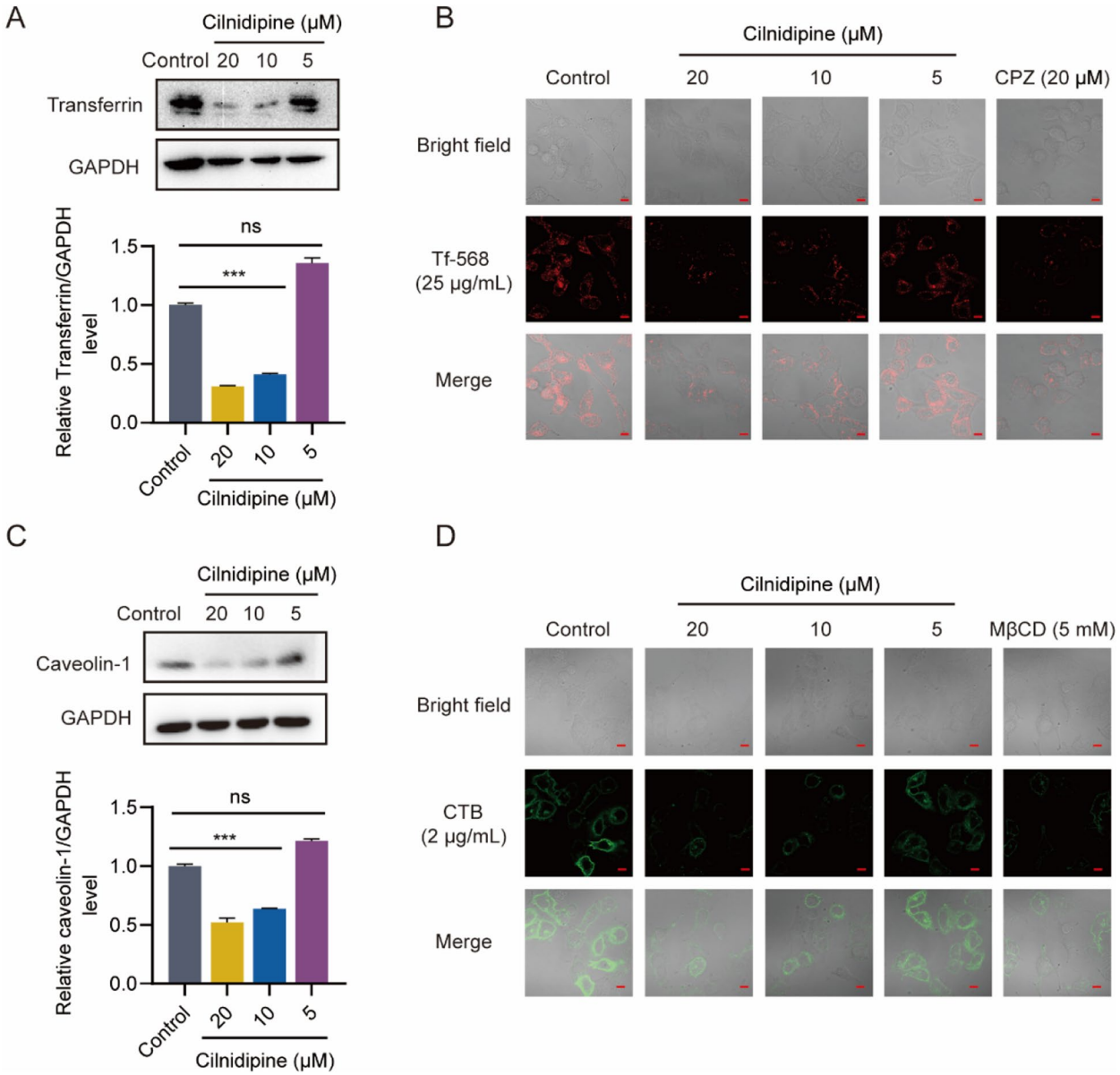

Fig. 3 Cilnidipine inhibits clathrin-mediated and caveolin-mediated endocytosis. **A** The inhibitory effect of cilnidipine on transferrin internalization was assessed via western blotting. **B** The effect of cilnidipine on the fluorescence expression of Tf-568 internalized in A549 cells was observed via confocal microscopy (400×). Scale bar: 10 μm. CPZ (20 μM) was used as positive control. **C** The inhibitory effect of cilnidipine on caveolin-1 expression was assessed via western blotting. **D** Confocal microscopy was used to observe the effect of cilnidipine on the fluorescence of internalized CTB in A549 cells (400×). Scale bar: 10 μm. MβCD (5 mM) was used as positive control. The data is presented as the means ± SDs, *** $p < 0.001$, ns means not significant

cilnidipine on caveolin-1 expression and caveolae-mediated endocytosis using cholera toxin B subunit (CTB) as a marker. Our results showed that cilnidipine suppressed the expression of caveolin-1 (Fig. 3C). Cells internalized CTB (2 μg/mL) with fluorescence concentrated around the nucleus; however, treatment with cilnidipine led to a decrease in CTB internalization, indicating inhibition of caveolae-mediated uptake (Fig. 3D).

Cilnidipine exerts antiviral effects by inhibiting the MAPK and PI3K-AKT pathways

Viral internalization, a critical phase in the viral life cycle, typically begins with the binding of viral surface proteins to host cell receptors, activating pathways that facilitate viral particle uptake. Upon infection with IAV, there was a significant increase in the expression of phosphorylated PI3K (p-PI3K) protein. However, treatment with

cilnidipine leads to a reduction in p-PI3K protein expression (Fig. 4A). Additionally, cilnidipine inhibited the phosphorylation of downstream Akt, which is induced by PI3K activation (Fig. 4A). Following viral infection, the MAPK signaling pathway plays a crucial role in regulating various cellular functions. Cilnidipine effectively inhibited the phosphorylation of p38 (p-p38) and the subsequent activation of the MAPK pathway induced by virus infection (Fig. 4B). Importantly, when cilnidipine is administered alone, in the absence of viral infection, it did not exert an inhibitory effect on these signaling pathways (Additional file 1: Fig. S8). Therefore, cilnidipine may inhibit viral entry into cells by modulating the virus-activated PI3K-Akt and p38 MAPK signaling pathways.

Cilnidipine exhibits significant anti-IAV infection effects in vivo

The in vivo anti-IAV efficacy of cilnidipine was assessed using a mouse model of acute lung injury (ALI). As shown in Fig. 5A, BALB/c mice were intranasally infected with the PR8 virus and orally administered cilnidipine at doses of 50, 25, or 12.5 mg/kg, oseltamivir (Ose) at 60 mg/kg, or 0.5% CMC as a vehicle control. Recognizing the hypotensive effects of cilnidipine, we monitored blood pressure changes in mice. Notably, cilnidipine administration had no notable impact on the blood pressure of treated mice (Fig. 5B). Lung morphology showed that cilnidipine mitigated severe pulmonary damage in IAV-infected mice (Fig. 5C). Histopathological assessments indicated that cilnidipine reduced alveolar exudation, alveolar wall destruction, and alveolar hemorrhage (Fig. 5D). These effects were comparable to those observed with Ose treatment. Furthermore, the impact of cilnidipine on viral titers in IAV-infected lungs was assessed through plaque assays and $TCID_{50}$, which revealed a significant reduction in the cilnidipine-treated groups (Fig. 5E and 5F). Cilnidipine also reduced the viral lung index (Fig. 5G) and NP mRNA expression (Fig. 5H). Furthermore, it significantly decreased the mRNA expression of IAV-induced pulmonary inflammatory cytokines, including IL-1β, TNF-α, IL-6, IFN-β, and IL-8 (F ig. 5I-M), indicating its inhibition of IAV infection in vivo.

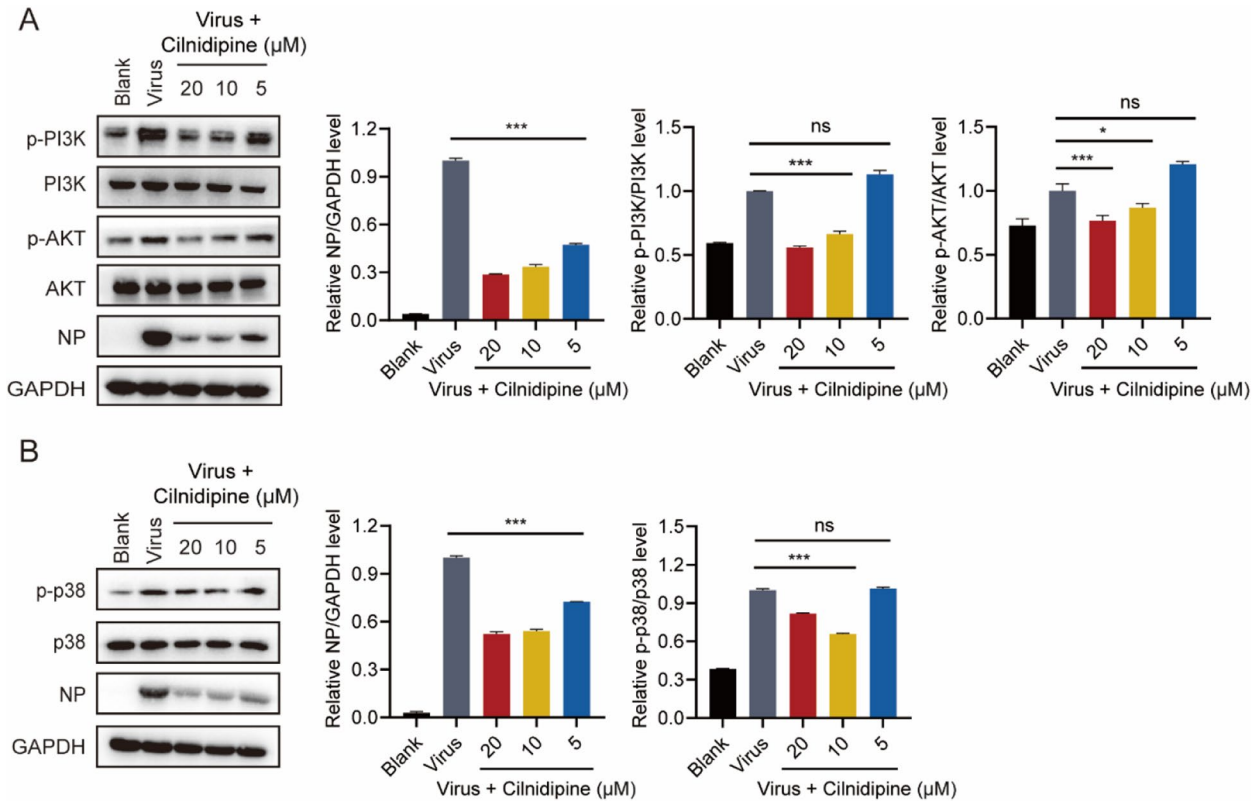

Fig. 4 Effect of cilnidipine on the MAPK and PI3K-AKT pathways activated by IAV infection. **A** The protein expression of phosphorylated PI3K (p-PI3K) and phosphorylated AKT (p-AKT) were detected via western blotting. **B** The protein expression of phosphorylated p38 (p-p38) was detected via western blotting. The data are presented as the means ± SDs, * $p < 0.05$, *** $p < 0.001$, ns means not significant

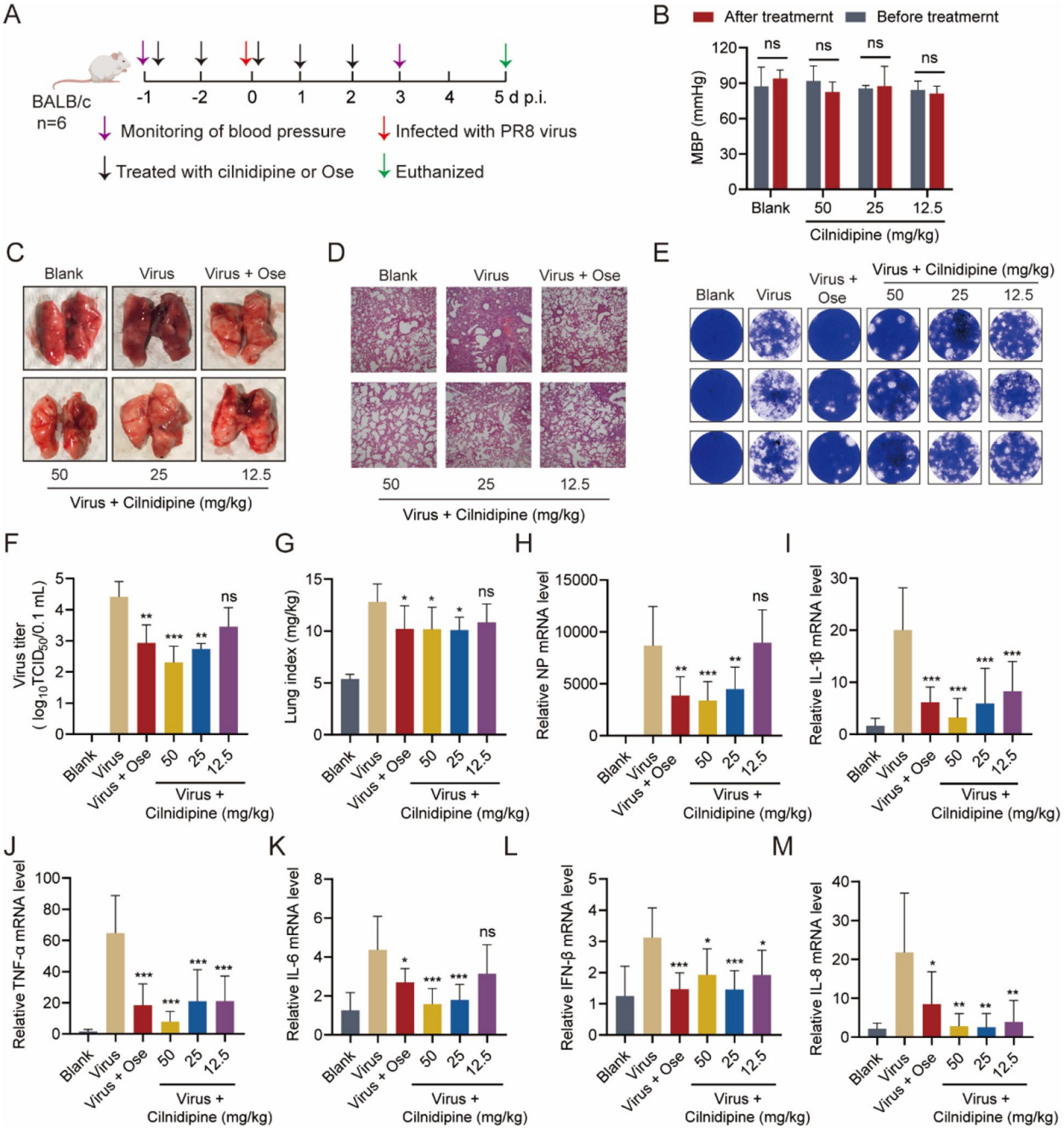

Fig. 5 The antiviral effect of cilnidipine against IAV in vivo. **A** The diagram depicts treatment with cilnidipine in BALB/c mice infected with the PR8 virus. **B** Blood pressure changes in cilnidipine-treated mice were monitored using noninvasive blood pressure measurement devices. **C** The macroscopic appearance of mice infected with IAV was observed. **D** Histological examination of lung tissues was performed using hematoxylin and eosin (H&E) staining to evaluate pathological changes. **E-F** Viral titers in the lungs of the mice were determined by plaque assay and Reed–Muench method, respectively. **G** Lung index. **H** Viral NP mRNA expression in mouse lung tissue homogenates was determined by qRT–PCR. **I-M** The mRNA expression levels of inflammatory cytokines IL-1β, TNF-α, IL-6, IFN-β, and IL-8 in lung tissues were detected by qRT-PCR. The data are presented as the means ± SDs, * $p < 0.05$, *** $p < 0.001$, ns means not significant

Cilnidipine exerts a protective effect on the survival of IAV-infected mice

After intranasal infection of BALB/c mice with the PR8 virus, changes in body weight and survival rates were observed for 14 days (Fig. 6A). The results shown in Fig. 6B indicated that the mice in the virus group

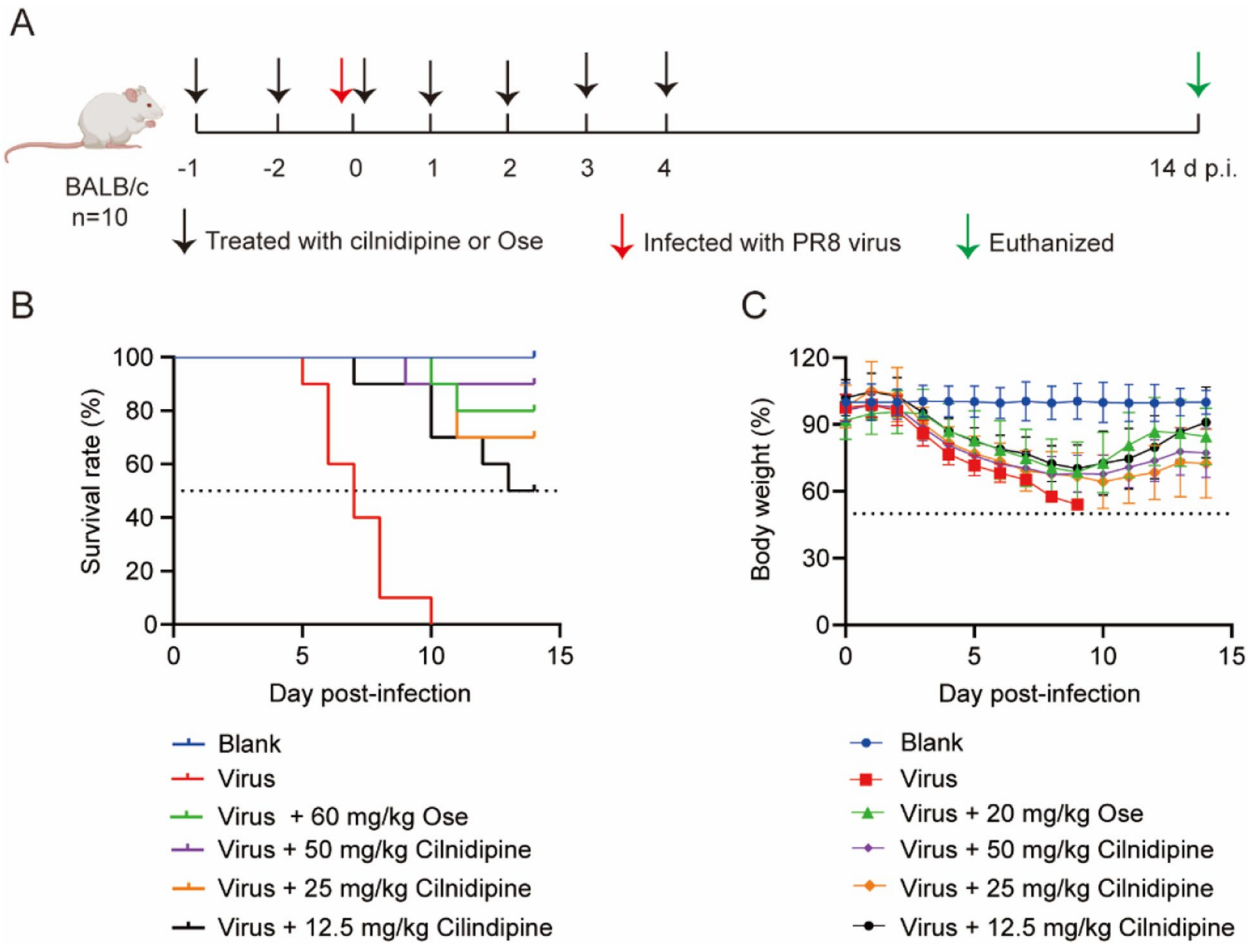

Fig. 6 Effects of cilnidipine on H1N1 infection-induced mortality and body weight changes in mice. **A** Schematic diagram of the survival protection of the mice. **B** The survival rate of mice 14 days post-infection was recorded. **C** The percentage of body weight loss in the mice 14 days post-infection was recorded

began to die at 5 d p.i., with all mice dying by 10 d.p.i.. Cilnidipine-treated groups exhibited a significant 2-day delay in mortality, with even the low-concentration group achieving a 50% survival rate. The high-dose cilnidipine group (50 mg/kg) presented a survival rate of 90%, surpassing the 80% survival rate observed in the Ose-treated group (Fig. 6B). Furthermore, the body weights of the virus-infected mice gradually decreased beginning at 3 d p.i., reaching their lowest point at 9 d p.i. (Fig. 6C). However, the administration of cilnidipine mitigated weight loss, and the mice began to regain weight after 9 d.p.i. (Fig. 6C). In summary, cilnidipine was effective in increasing survival rates and alleviating symptoms associated with the infection, such as lethargy, ruffled fur, and weight loss.

Discussion

The emergence of IAV variants and increased breakthrough infections in vaccinated populations highlight an urgent need for new antiviral drugs. Repurposing approved medications is a vital strategy for rapid drug development, as demonstrated in the COVID-19 pandemic [36]. For example, fluvoxamine, a selective serotonin reuptake inhibitor (SSRI) antidepressant, has shown significant efficacy in early SARS-CoV-2 infection, reducing hospitalization risk in high-risk COVID-19 patients [37, 38]. Previous research conducted in our laboratory revealed that the antidepressant drug sertraline binds to the receptor binding domain (RBD) of the SARS-CoV-2 S protein, thereby impeding its interaction with hACE2 [39]. Moreover, clopidogrel, which reduces

cerebrovascular disease risk, and triamterene, a diuretic, have exhibited inhibitory effects on various IAV subtypes [40]. These findings indicate that approved drugs may offer innovative adjunctive therapies against influenza infection.

Targeting host cells is an attractive strategy against influenza virus, which is prone to developing drug resistance. Research has shown that alterations in host cell Ca^{2+} levels are crucial for IAV infection. IAV binding to Ca^{2+} channel proteins triggers Ca^{2+} influx, facilitating viral entry and infection, and knocking out these proteins inhibits IAV-induced Ca^{2+} currents and infection [24]. CCBs, such as cilnidipine, are commonly used to manage hypertension and cardiovascular conditions by inhibiting Ca^{2+} channels that regulate smooth muscle contractility in peripheral arteries. Cilnidipine, which affects both L-type and N-type Ca^{2+} channels, has demonstrated antiviral activity by hindering the entry of hantaviruses in vitro and eliminating West Nile virus (WNV) infection in Vero cells and human neuroblastoma SH-SY5Y cells [41, 42]. It also exhibits broad-spectrum antiviral activity against viruses like Zika, Japanese encephalitis, yellow fever, tick-borne encephalitis, and chikungunya [42]. Our study reveals the in vitro and in vivo antiviral effects of cilnidipine, as well as its dual antiviral mechanism of inhibiting viral internalization and targeting the viral HA2 subunit to prevent viral entry. Therefore, we propose cilnidipine as a promising antiviral agent for combating influenza viruses, with potential for clinical application.

The MTT assay revealed that cilnidipine exhibited a dose-dependent inhibitory effect on various IAV subtypes, including oseltamivir-resistant strains, with minimal cytotoxicity and a high safety index. Additionally, cilnidipine significantly reduced the expression of viral NP protein and mRNA, decreased viral progeny titers, and protected cells from virus-induced CPE, demonstrating effective antiviral activity in vitro. The influenza virus life cycle, spanning approximately 8–10 h, includes viral entry (0–2 h), transcription and replication of viral genes (2–8 h), and release of progeny virions (8–10 h) [34]. Subsequent time-of-addition assays were conducted to determine the specific stage of the viral life cycle targeted by cilnidipine. The results demonstrated that cilnidipine, as an entry inhibitor, potentially exerts its effects during the stages of viral attachment, internalization into endosomes, and the fusion of the viral envelope with the endosomal membrane. Treatment with NH_4Cl rapidly increases the pH to 6.7, decelerating the entry of viral particles into secondary lysosomes, and thus allowing for the investigation of viral binding and internalization processes [43]. Cilnidipine effectively suppressed NP mRNA expression in the presence of NH_4Cl, indicating potential inhibition of the stage preceding membrane fusion. Our study indicated that cilnidipine treatment did not reduce virus binding but significantly reduced IAV internalization. Direct viral membrane fusion assays at low pH confirmed that cilnidipine requires the internalization phase to exert its antiviral activity. Previous studies have firmly established CME and caveolin-mediated endocytosis as crucial pathways facilitating influenza virus entry into host cells [32, 44]. To investigate the effect of cilnidipine on CME, we utilized transferrin as a specific marker and employed both western blotting and fluorescence confocal microscopy. Cilnidipine effectively hinders transferrin uptake and disrupts CME, with CPZ (chlorpromazine) serving as a positive control that inhibits coated pit formation on the cell surface, thereby impeding CME [45, 46]. Additionally, caveolae, enriched with cholesterol, glycosphingolipids, and caveolin (a 20–24 kDa membrane protein), play a pivotal role in the internalization of various viruses [47, 48]. Notably, cilnidipine suppressed the expression caveolin-1 and inhibited the internalization of CTB, which specifically interacts with caveolae via its ganglioside GM1 receptor [49]. This inhibitory effect was comparable to that observed with MβCD, a positive control that disrupts the lipid raft structure essential for CTB internalization. These results suggest that cilnidipine may inhibit viral internalization by suppressing clathrin- and caveolae-mediated endocytosis. Cilnidipine also showed dose-dependent inhibition of H5N1 pseudovirus activity, suggesting a potential influence on viral HA and NA proteins. The results demonstrated that cilnidipine did not inhibit NA activity or the function of the HA1 subunit, but rather it inhibited syncytium formation induced by the HA2 subunit. Furthermore, SPR assays further confirmed that cilnidipine had bound directly to the HA2 protein.

Upon attaching to host cells, viruses initiate signaling cascades, particularly the PI3K-AKT and p38 MAPK pathways, which are essential for viral entry. Research has shown that various viruses, including IAV, Herpes Simplex Virus Type 1 (HSV-1) [50], Ebola Virus (EBoV) [51], and Avian Leukosis Virus (ALV) [52], activate the PI3K-AKT signaling pathway to facilitate entry into host cells. Early in the viral cycle, the PI3K-Akt signaling pathway is hijacked by the influenza virus to facilitate viral entry [53]. Specifically, IAV interaction with sialic acid receptors induces lipid raft aggregation and activates receptor tyrosine kinases (RTKs) [54], triggering a PI3K-AKT pathway cascade that stimulates virus entry through clathrin-independent endocytosis [55]. Inhibition of this cascade can prevent viral internalization, sequestering viral particles in vesicular compartments and halting intracellular transport [56]. Our findings indicate that cilnidipine inhibits virus-induced

PI3K phosphorylation and subsequent AKT activation, blocking viral entry. The p38 MAPK pathway also regulates viral endocytosis and contributes to viral entry. Studies have shown that Toll-like receptor 4-mediated activation of p38 mitogen-activated protein kinase is a determinant of respiratory virus entry and tropism [57]. The inhibitory effect of cilnidipine on the p38 MAPK pathway could significantly impede viral endocytosis, thereby disrupting the initial stages of viral infection. In summary, cilnidipine exerts its antiviral activity by inhibiting the virus-induced activation of the PI3K-AKT and p38 MAPK signaling pathways, disrupting key cellular mechanisms required for viral entry. These signaling pathways not only mediate viral entry but also modulate the host immune response. Thus, inhibition of these pathways by cilnidipine may enhance host antiviral defenses by blocking viral entry and modulating the immune response. Excessive accumulation of Ca^{2+} can result in the accumulation of mitochondrial reactive oxygen species (mtROS), thereby exacerbating cellular damage. Additionally, we investigated the impact of cilnidipine on IAV-induced intracellular Ca^{2+} concentration and oxygen species (ROS) levels. The results demonstrated that cilnidipine exhibited inhibitory effects on virus-induced increases in calcium levels (Additional file 1: Fig. S9), reduced ROS production (Additional file 1: Fig. S10), and alleviated mitochondrial stress.

Based on the in vitro antiviral efficacy, we assessed the in vivo antiviral efficacy of cilnidipine by intranasally infecting BALB/c mice with the PR8 virus to induce viral pneumonia. Parameters such as the lung index, lung pathology, viral load, and levels of inflammatory mediators in the lung were utilized as reliable indicators for assessing the effectiveness of pharmaceutical interventions against IAV. Treatment with cilnidipine was found to ameliorate these symptoms and increase the survival rate of mice afflicted with viral pneumonia. In addition, we evaluated blood pressure levels in mice before and after the oral administration of cilnidipine. The results showed that cilnidipine did not affect blood pressure, indicating that its antiviral activity is likely due to direct interactions with viral entry mechanisms, not cardiovascular side effects. The stability of blood pressure observed with cilnidipine reduces the risk of hypotension, making it a feasible choice for patients with cardiovascular conditions. Collectively, the minimal impact of cilnidipine on blood pressure underscores its specificity and safety profile, rendering it a promising antiviral agent for treating infections where cardiovascular stability is paramount.

In this study, we identified multiple mechanisms by which cilnidipine inhibits influenza virus infection, highlighting its potential as an important therapeutic option for influenza patients. Future research will focus on elucidating how cilnidipine modulates the internal environment of the host to combat viral infections.

Conclusions

Overall, our research demonstrated the inhibitory effects of cilnidipine on IAV both in vivo and in vitro. Cilnidipine effectively impedes IAV internalization by blocking both clathrin-mediated and caveolin-mediated endocytosis, as well as by targeting the HA2 subunit to hinder viral membrane fusion. Additionally, it also regulates the virus-activated PI3K-AKT and p38 MAPK pathways, which are critical for viral entry.

Abbreviations

ALI	Acute lung injury
CPE	Cytopathic effect
Ca^{2+}	Calcium ion
CCBs	Calcium channel blockers
CC_{50}	50% Cytotoxic concentration
CTB	Cholera toxin subunit B
DMEM	Dulbecco's modified Eagle's medium
d p.i	Days post–infection
H&E	Hematoxylin–eosin
h p.i.	Hours post–infection
HA	Hemagglutinin
IAV	Influenza A virus
IC_{50}	50% Inhibitory concentration
MU-NANA	2′-(4-Methylumbelliferyl)-D-N-acetylneuraminic acid
MOI	Multiplicity of infection
MTT	3-(4,5-Dimethylthiazol-2-yl)-2,5-diphenyltetrazolium bromide
MAPK	Mitogen-activated protein kinase
MβCD	Methyl-β-cyclodextrin
NA	Neuraminidase
NAIs	Neuraminidase inhibitors
PI3K	Phosphatidylinositol 3-kinase
$TCID_{50}$	50% Tissue culture infection dose
vRNPs	Viral ribonucleoprotein complex
WSN	A/WSN/1933(H1N1)

Supplementary Information

The online version contains supplementary material available at https://doi.org/10.1186/s12916-025-04022-0.

Additional file 1: Figure S1. Schematic of the time-of-addition. Figure S2. Cilnidipine does not inhibit viral NP expression at 4°C. Figure S3. EDTA-trypsin treatment reduces viral NP levels, indicating the removal of non-internalized virus. Figure S4. CL-385319 inhibits H5N1 pseudovirus infection in MDCK cells. Figure S5. Cilnidipine does not exhibit inhibitory effects on neuraminidaseactivity. Figure S6. Cilnidipine does not inhibit IAV-induced cRBC aggregation. Figure S7. Cilnidipine does not exhibit inhibitory effects on the polymerase activity as determined by mini-replicon assay. Figure S8. The direct impacts of cilnidipine on the PI3K-AKT and p38 MAPK signaling pathways. Figure S9. Cilnidipine inhibits intracellular Ca^{2+} concentration. Figure S10. Cilnidipine inhibits ROS activity.

Additional file 2: Original images of western blots in Fig. 1B, Fig. 2A, Fig. 2D, Fig. 2E, Fig. 3A, Fig. 3C, Fig. 4A and Fig. 4B.

Acknowledgements

We thank BioRender (https://app.biorender.com/) and Ranke Biotech Co.,Ltd. (Guangzhou, China) for providing us with the drawing material.

Authors' contributions
All authors substantially contributed to this study. YYL, SZY, FJ, XC, and JY played a key role in the conception, design, and execution of the study. JY obtained funding. YYL, SZY, and FJ performed in vitro and in vivo antiviral assays, while YYL, SQL, JLL, LRJ, and ZXC investigated the antiviral mechanisms. YYL used software for data acquisition and analysis. YYL and JY drafted the manuscript, which JY and XC reviewed. All authors approved the final manuscript.

Funding
This research was funded by the National Natural Science Foundation of China (Grant numbers 82470030 and 82373915).

Data availability
Data is available from the corresponding authors upon reasonable request.

Declarations

Ethics approval and consent to participate
Animal experiments were performed in a biosafety level 2 animal laboratory according to animal welfare and related regulations about lab activities as described in the Directory of Pathogenic Microorganisms Transmitted among Humans issued by the Chinese Ministry of Health. The National Institutional Animal Care and Medical Ethics Committee of Southern Medical University approved the experiments reported in this study (Approval number: SMUL202408006).

Consent for publication
Not applicable. This study did not involve human participants.

Competing interests
The authors declare no competing interests.

Received: 20 November 2024 Accepted: 19 March 2025
Published online: 07 April 2025

References

1. Lewis DB. Avian flu to human influenza. Annu Rev Med. 2006;57:139–54.
2. Krammer F, Smith GJD, Fouchier RAM, Peiris M, Kedzierska K, Doherty PC, et al. Influenza Nat Rev Dis Primers. 2018;4(1):3.
3. Webster RG, Govorkova EA. Continuing challenges in influenza. Ann N Y Acad Sci. 2014;1323(1):115–39.
4. Bai L, Cao B, Wang C. Influenza A pandemic (H1N1) 2009 virus infection. Chin Med J (Engl). 2011;124(20):3399–402.
5. Su S, Gu M, Liu D, Cui J, Gao GF, Zhou J, et al. Epidemiology, evolution, and pathogenesis of H7N9 influenza viruses in five epidemic waves since 2013 in China. Trends Microbiol. 2017;25(9):713–28.
6. Charostad J, Rezaei Zadeh Rukerd M, Mahmoudvand S, Bashash D, Hashemi SMA, Nakhaie M,et al. A comprehensive review of highly pathogenic avian influenza (HPAI) H5N1: An imminent threat at doorstep. Travel Med Infect Dis. 2023;55:102638.
7. de Francisco SN, Donadel M, Jit M, Hutubessy R. A systematic review of the social and economic burden of influenza in low- and middle-income countries. Vaccine. 2015;33(48):6537–44.
8. Nypaver C, Dehlinger C, Carter C. Influenza and Influenza Vaccine: A Review. J Midwifery Womens Health. 2021;66(1):45–53.
9. Loregian A, Mercorelli B, Nannetti G, Compagnin C, Palù G. Antiviral strategies against influenza virus: towards new therapeutic approaches. Cell Mol Life Sci. 2014;71(19):3659–83.
10. Kumari R, Sharma SD, Kumar A, Ende Z, Mishina M, Wang Y, et al. Antiviral Approaches against Influenza Virus. Clin Microbiol Rev. 2023;36(1): e0004022.
11. Samson M, Pizzorno A, Abed Y, Boivin G. Influenza virus resistance to neuraminidase inhibitors. Antiviral Res. 2013;98(2):174–85.
12. Dharan NJ, Gubareva LV, Meyer JJ, Okomo-Adhiambo M, McClinton RC, Marshall SA, et al. Infections with oseltamivir-resistant influenza A(H1N1) virus in the United States. JAMA. 2009;301(10):1034–41.
13. Lackenby A, Moran Gilad J, Pebody R, Miah S, Calatayud L, Bolotin S, et al. Continued emergence and changing epidemiology of oseltamivir-resistant influenza A(H1N1)2009 virus, United Kingdom, winter 2010/11. Euro Surveill. 2011;16(5):19784.
14. Shirley M. Baloxavir Marboxil: a review in acute uncomplicated Influenza. Drugs. 2020;80(11):1109–18.
15. Hickerson BT, Petrovskaya SN, Dickensheets H, Donnelly RP, Ince WL, Ilyushina NA. Impact of baloxavir resistance-associated substitutions on influenza virus growth and drug susceptibility. J Virol. 2023;97(7): e0015423.
16. Yang J, Liu S. Influenza Virus Entry inhibitors. Adv Exp Med Biol. 2022;1366:123–35.
17. Xiu S, Dick A, Ju H, Mirzaie S, Abdi F, Cocklin S, et al. Inhibitors of SARS-CoV-2 Entry: Current and Future Opportunities. J Med Chem. 2020;63(21):12256–74.
18. Kuritzkes DR. HIV-1 entry inhibitors: an overview. Curr Opin HIV AIDS. 2009;4(2):82–7.
19. Luo M. Influenza virus entry. Adv Exp Med Biol. 2012;726:201–21.
20. Eisfeld AJ, Neumann G, Kawaoka Y. At the centre: influenza A virus ribonucleoproteins. Nat Rev Microbiol. 2015;13(1):28–41.
21. Dou D, Revol R, Östbye H, Wang H, Daniels R. Influenza A virus cell entry, replication, virion assembly and movement. Front Immunol. 2018;9:1581.
22. Chen X, Cao R, Zhong W. Host calcium channels and pumps in viral infections. Cells. 2019;9(1):94.
23. Zhou Y, Frey TK, Yang JJ. Viral calciomics: interplays between Ca^{2+} and virus. Cell Calcium. 2009;46(1):1–17.
24. Fujioka Y, Nishide S, Ose T, Suzuki T, Kato I, Fukuhara H, et al. A sialylated voltage-dependent Ca^{2+} channel binds hemagglutinin and mediates influenza A virus entry into mammalian cells. Cell Host Microbe. 2018;23:809–18.
25. Li H, Zhang LK, Li SF, Zhang SF, Wan WW, Zhang YL, et al. Calcium channel blockers reduce severe fever with thrombocytopenia syndrome virus (SFTSV) related fatality. Cell Res. 2019;29:739–53.
26. Wang X, Luo J, Wen Z, Shuai L, Wang C, Zhong G, et al. Diltiazem inhibits SARS-CoV-2 cell attachment and internalization and decreases the viral infection in mouse lung. PLoS Pathog. 2022;18(2): e1010343.
27. Pizzorno A, Terrier O, Nicolas de Lamballerie C, Julien T, Padey B, Traversier A,et al. Repurposing of drugs as novel influenza inhibitors from clinical gene expression infection signatures. Front Immunol. 2019;10:60–77.
28. Nugent KM, Shanley JD. Verapamil inhibits influenza A virus replication. Arch Virol. 1984;81:163–70.
29. Reed LJ, Muench H. A simple method of estimating fifty percent endpoints. Am J Epidemiol. 1938;27(3):493–7.
30. Liu S, Li R, Zhang R, Chan CC, Xi B, Zhu Z, et al. CL-385319 inhibits H5N1 avian influenza A virus infection by blocking viral entry. Eur J Pharmacol. 2011;660:460–7.
31. Hybiske K, Stephens RS. Mechanisms of Chlamydia trachomatis entry into nonphagocytic cells. Infect Immun. 2007;75(8):3925–34.
32. Sieczkarski SB, Whittaker GR. Influenza virus can enter and infect cells in the absence of clathrin-mediated endocytosis. J Virol. 2002;76:10455–64.
33. Huang Y, Li Y, Chen Z, Chen L, Liang J, Zhang C, et al. Nisoldipine inhibits influenza A virus infection by interfering with virus internalization process. Viruses. 2022;14(12):2738.
34. Yu M, Si L, Wang Y, Wu Y, Yu F, Jiao P, et al. Discovery of pentacyclic triterpenoids as potential entry inhibitors of influenza viruses. J Med Chem. 2014;57(23):10058–71.
35. Li Y, Sang H, Mo Q, Jiang L, Chen Z, Liang J, et al. Cepharanthine inhibits influenza A virus replication by impairing viral polymerase activity and regulating influenza-induced immune response. Phytomedicine Plus. 2024;4(2): 100553.
36. Ng YL, Salim CK, Chu JJH. Drug repurposing for COVID-19: Approaches, challenges and promising candidates. Pharmacol Ther. 2021;228: 107930.
37. Facente SN, Reiersen AM, Lenze EJ, Boulware DR, Klausner JD. Fluvoxamine for the Early Treatment of SARS-CoV-2 Infection: A Review of Current Evidence. Drugs. 2021;81(18):2081–9.
38. Hashimoto Y, Suzuki T, Hashimoto K. Mechanisms of action of fluvoxamine for COVID-19: a historical review. Mol Psychiatry. 2022;27(4):1898–907.

39. Chen Y, Wu Y, Chen S, Zhan Q, Wu D, Yang C, et al. Sertraline is an effective SARS-CoV-2 entry inhibitor targeting the spike protein. J Virol. 2022;96(24): e0124522.
40. Orr-Burks N, Murray J, Todd KV, Bakre A, Tripp RA. Drug repositioning of Clopidogrel or Triamterene to inhibit influenza virus replication in vitro. PLoS ONE. 2021;16(10): e0259129.
41. Wang B, Pei J, Zhang H, Li J, Dang Y, Liu H, et al. Dihydropyridine-derived calcium channel blocker as a promising anti-hantavirus entry inhibitor. Front Pharmacol. 2022;13: 940178.
42. Tang H, Liu Y, Ren R, Liu Y, He Y, Qi Z, et al. Identification of clinical candidates against West Nile virus by activity screening in vitro and effect evaluation in vivo. J Med Virol. 2022;94(10):4918–25.
43. Yoshimura A, Ohnishi S. Uncoating of influenza virus in endosomes. J Virol. 1984;51:497–504.
44. de Vries E, Tscherne DM, Wienholts MJ, Cobos-Jiménez V, Scholte F, García-Sastre A, et al. Dissection of the influenza A virus endocytic routes reveals macropinocytosis as an alternative entry pathway. PLoS Pathog. 2011;7(3): e1001329.
45. Wang S, Huang X, Huang Y, Hao X, Xu H, Cai M, et al. Entry of a novel marine DNA virus, Singapore grouper iridovirus, into host cells occurs via clathrin-mediated endocytosis and macropinocytosis in a pH-dependent manner. J Virol. 2014;88(22):13047–63.
46. Hernaez B, Alonso C. Dynamin- and clathrin-dependent endocytosis in African swine fever virus entry. J Virol. 2010;84(4):2100–9.
47. Pelkmans L, Kartenbeck J, Helenius A. Caveolar endocytosis of simian virus 40 reveals a new two-step vesicular-transport pathway to the ER. Nat Cell Biol. 2001;3(5):473–83.
48. Martinez MG, Cordo SM, Candurra NA. Characterization of Junin arenavirus cell entry. J Gen Virol. 2007;88(Pt 6):1776–84.
49. Pietiäinen V, Marjomäki V, Upla P, Pelkmans L, Helenius A, Hyypiä T. Echovirus 1 endocytosis into caveosomes requires lipid rafts, dynamin II, and signaling events. Mol Biol Cell. 2004;15(11):4911–25.
50. Cheshenko N, Trepanier JB, Stefanidou M, Buckley N, Gonzalez P, Jacobs W, et al. HSV activates Akt to trigger calcium release and promote viral entry: novel candidate target for treatment and suppression. FASEB J. 2013;27(7):2584–99.
51. Saeed MF, Kolokoltsov AA, Freiberg AN, Holbrook MR, Davey RA. Phosphoinositide-3 kinase-Akt pathway controls cellular entry of Ebola virus. PLoS Pathog. 2008;4(8): e1000141.
52. Feng SZ, Cao WS, Liao M. The PI3K/Akt pathway is involved in early infection of some exogenous avian leukosis viruses. J Gen Virol. 2011;92(Pt 7):1688–97.
53. Blanco J, Cameirao C, López MC, Muñoz-Barroso I. Phosphatidylinositol-3-kinase-Akt pathway in negative-stranded RNA virus infection: a minireview. Arch Virol. 2020;165(10):2165–76.
54. Lakadamyali M, Rust MJ, Zhuang X. Endocytosis of influenza viruses. Microbes Infect. 2004;6(10):929–36.
55. Fujioka Y, Tsuda M, Hattori T, Sasaki J, Sasaki T, Miyazaki T, et al. The Ras-PI3K signaling pathway is involved in clathrin-independent endocytosis and the internalization of influenza viruses. PLoS ONE. 2011;6(1): e16324.
56. Diehl N, Schaal H. Make yourself at home: viral hijacking of the PI3K/Akt signaling pathway. Viruses. 2013;5(12):3192–212.
57. Marchant D, Singhera GK, Utokaparch S, Hackett TL, Boyd JH, Luo Z, et al. Toll-like receptor 4-mediated activation of p38 mitogen-activated protein kinase is a determinant of respiratory virus entry and tropism. J Virol. 2010;84(21):11359–73.

Publisher's Note